JOURNAL OF COMPUTATIONAL PHYSICS **140,** 432–452 (1998)
ARTICLE NO. CP985893

The Adjoint Method for an Inverse Design Problem in the Directional Solidification of Binary Alloys

George Z. Yang and Nicholas Zabaras

Sibley School of Mechanical and Aerospace Engineering, 188 Frank H. T. Rhodes Hall, Cornell University, Ithaca, New York 14853-3801
E-mail: zabaras@sofia.mae.cornell.edu, njz1@cornell.edu

Received June 30, 1997; revised December 9, 1997

This paper presents a systematic procedure based on the adjoint method for solving a class of inverse directional alloy solidification design problems in which a desired growth velocity $\boldsymbol{v}_f$ is achieved under stable growth conditions. To the best of our knowledge, this is the first time that a continuum adjoint formulation is proposed for the solution of an inverse problem with simultaneous heat and mass transfer, thermo-solutal convection, and phase change. In this paper, the interfacial stability is considered to imply a sharp solid–liquid freezing interface. This condition is enforced using the constitutional undercooling criterion in the form of an inequality constraint between the thermal and solute concentration gradients, G and G_c, respectively, at the freezing front. The main unknowns of the design problem are the heating and/or cooling boundary conditions on the mold walls. The inverse design problem is formulated as a functional optimization problem. The cost functional is defined by the square of the L_2 norm of the deviation of the freezing interface temperature from the temperature corresponding to thermodynamic equilibrium. A continuum adjoint system is derived to calculate the adjoint temperature, concentration, and velocity fields such that the gradient of the cost functional can be expressed analytically. The cost functional minimization process is realized by the conjugate gradient method via the finite element method solutions of the continuum direct, sensitivity, and adjoint problems. The developed formulation is demonstrated with an example of designing the directional solidification of a binary aqueous solution in a rectangular mold such that a stable vertical interface advances from left to right with a desired growth velocity.

Key Words: inverse problems; design problems; adjoint method; functional optimization; conjugate gradient method; binary alloy solidification; constitutional undercooling; double diffusive convection; finite element method.

0021-9991/98 $25.00

1. INTRODUCTION

Various design, identification, and control problems take the form of an *inverse problem* in which, in addition to the various field equations, incomplete conditions are available in part of the boundary, whereas overspecified boundary conditions are supplied in another part of the boundary [1–3].

Significant attention has been given to conduction based inverse heat transfer problems [4–6]. Applications to solidification processes were also addressed [7–11]. Time sequential as well as whole time domain solution techniques have been developed including finite and infinite-dimensional optimization schemes [4, 5, 9, 12].

Some attention has also been given to inverse heat transfer problems involving free or forced convection [13–16]. In our recent work [17], we derived a functional optimization formulation and continuum adjoint equations for inverse natural convection problems. This work was recently extended to the inverse design of solidification of pure substances with a desired interface heat flux G and growth velocity $\boldsymbol{v}_f$ [18]. The combination of G and $\boldsymbol{v}_f$ has important implications on the type and scale of the obtained solidification microstructures [19].

This paper will generalize our earlier analysis to the inverse design of directional solidification processes of dilute binary alloys. Heat and mass transfer and melt flow are the key transport mechanisms in the solidification of binary alloys. In addition, one must consider the phase change process at the solid–liquid freezing interface. For a dilute binary alloy, a macroscopic sharp solid–liquid freezing interface can exist at thermodynamic equilibrium at the liquidus temperature corresponding to the interface concentration as dictated by the phase diagram. Assuming a macroscopically sharp interface, a *well posed direct mathematical model* of alloy solidification can then be defined for the calculation of the temperature, concentration, and flow fields, as well as for the calculation of the interface shape and growth. The temperature (or heat flux) on the whole mass impermeable mold boundary is assumed to be known in this direct model.

Although the above-stated mathematical direct problem is well posed, there is no guarantee that its solution will satisfy the *a-priori assumption* of a sharp solid–liquid interface. Such inconsistencies between the analytical model and the physical experiment have been reported in [20]. One of the most simplified necessary conditions for the existence of the sharp solid–liquid front in binary alloy solidification is the absence of *constitutional undercooling* in the liquid melt ahead of the freezing interface [19]. For the purpose of the present inverse design analysis, we will consider that the absence of constitutional undercooling is sufficient for the existence of a stable growth. A comprehensive review of morphological stability in solidification is given in [21].

The structure of this paper is as follows. At first, a *reference design directional solidification problem* with a desired growth and an a-priori assumption of a sharp freezing front is presented. Through a direct analysis it is shown that such a mathematical design is inconsistent with the corresponding physical model and that it eventually leads to an unstable interface growth. A precise definition of an *inverse design directional alloy solidification problem* is then presented in order to obtain a *desired stable growth* for a binary alloy system. The problem results in two separable inverse problems, one in the solid phase and another in the liquid melt. Emphasis is here given to the inverse problem in the liquid phase. The developed methodology is finally tested with an example problem in the solidification of a NH_4Cl water solution in a rectangular mold.

2. DEFINITION OF THE DIRECT PROBLEM AND OF A REFERENCE DESIGN PROBLEM

2.1. *The Direct Binary Alloy Solidification Problem*

Let us consider a directional solidification process of a dilute binary alloy that is confined in mass impermeable mold walls (see Fig. 1a). Initially the alloy melt is at a uniform concentration c_o and a uniform temperature T_i. At time $t = 0^+$, a cooling heat flux is applied at the side Γ_{os} of the mold wall to bring the boundary temperature to the freezing temperature corresponding to concentration c_o.

Let us denote the solid region as Ω_s and the liquid region as Ω_ℓ. These regions share the common interface boundary Γ_I whose normal vector $\boldsymbol{n}$ is defined pointing towards the solid region. The region Ω_ℓ has a boundary Γ_ℓ which consists of Γ_I (the solid–liquid interface), $\Gamma_{o\ell}$ (the vertical mold wall on the liquid side), and the remaining boundary $\Gamma_{h\ell}$ (the top and bottom horizontal mold walls). Similarly, Ω_s has boundary Γ_s, which includes Γ_I, Γ_{os}, and Γ_{hs}. The regions Ω_ℓ and Ω_s are time dependent and the interface Γ_I is moving to the right with a nonuniform velocity $\boldsymbol{v}_f$. Subscripts s and ℓ are used to denote quantities for the solid and liquid phases, respectively, while the subscript f is used to denote the freezing front.

We make the following assumptions about the transport of heat, solute, and momentum in the solidification system:

- Constant thermo-physical and transport properties, including thermal and solute diffusivities α and D, respectively, viscosity ν, density ρ, thermal conductivity k, and latent heat L.

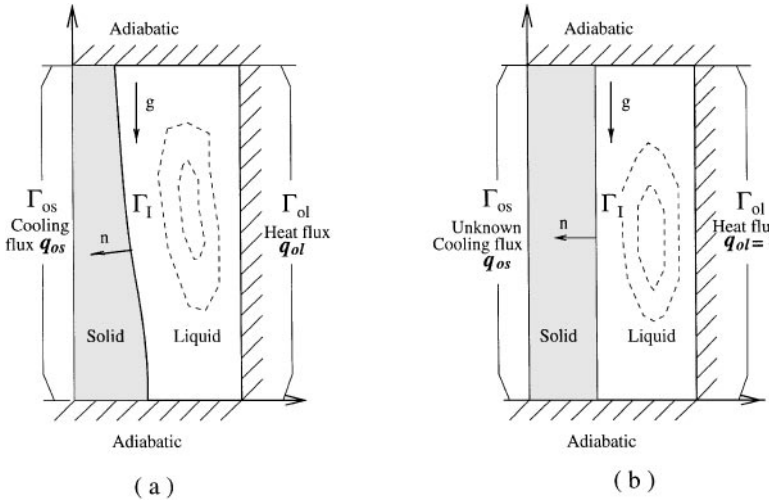

FIG. 1. Schematic of the *reference problem* of binary alloy solidification in a rectangular cavity: (a) the direct solidification problem with heat flux q_{os} (cooling) on the solid wall Γ_{os} and heat flux q_{ol} on the liquid mold wall. Solidification is assumed to proceed from the left to the right. For arbitrary q_{os} and q_{ol}, the effects of convection will lead to a curved interface as shown. (b) The *reference inverse design problem* to achieve a flat solid–liquid interface growth with a uniform desired velocity ($q_{ol} = 0$). The heat flux q_{os} is appropriately selected using an inverse heat conduction analysis. In both problems, an a-priori assumption of a stable growth (sharp solid/liquid interface) is made.

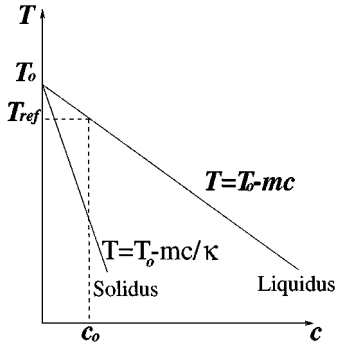

FIG. 2. Phase diagram of a dilute binary alloy: m is the magnitude of the slope of the liquidus line, κ is the partition ratio and T_o is the y-intercept of the solidus/liquidus line.

- The melt flow is assumed to be a laminar convective flow induced by temperature and concentration-dependent density variations subjected to the Boussinesq buoyancy forces (constant thermal and solute expansion coefficients β_T and β_C).
- The solute diffusion in the solid is negligible compared to that of the liquid, i.e. $D_s/D_\ell \to 0$.
- A macroscopically stable sharp interface exists between the solid and liquid regions.

The first two assumptions will generally be valid for solidification systems with dilute concentration level, moderate temperature differences, and a Newtonian liquid melt. The third assumption is true for most semiconductor materials and crystallized aqueous solutions. The existence of a sharp solid–liquid interface (last assumption) is nontrivial and does not necessarily conform with the physical reality corresponding to the prescribed cooling/heating boundary conditions. More discussion on the validity of the sharp interface assumption will be given in Section 2.2 with an example problem.

Let us introduce the dimensionless form of the governing equations. The reference temperature is taken as $T_{ref} = T_o - mc_o$, the length scale as l, and the time scale as l^2/α_ℓ. The parameters T_o and m are defined in Fig. 2. The following nondimensionalization of space, time, temperature, velocity, concentration, and pressure is introduced:

$$\bar{\boldsymbol{x}} = \frac{\boldsymbol{x}}{l}, \quad \bar{t} = \frac{\alpha_\ell t}{l^2}, \quad \bar{T} = \frac{T - T_{ref}}{T_i - T_{ref}}, \quad \bar{\boldsymbol{u}} = \frac{\boldsymbol{u}l}{\alpha_\ell}, \quad \bar{c} = \frac{c_o - c}{\gamma c_o}, \quad \bar{p} = \frac{pl^2}{\rho\alpha_\ell^2}, \tag{1}$$

where $\gamma = 1 + (T_i - T_o)/mc_o$ indicates the relative amount of initial super-heating of the liquid melt. We introduce the following familiar nondimensional parameters Pr, Le, Ra_T, Ra_C, and Ste [17]. In the rest of this paper, we will drop the overline "-" in the notation of the nondimensional quantities and all quantities shown are dimensionless unless it is otherwise stated. The nondimensional governing equations take the form

$$\frac{\partial T(\boldsymbol{x}, t; q_o)}{\partial t} + \boldsymbol{u}(\boldsymbol{x}, t; q_o) \cdot \nabla T(\boldsymbol{x}, t; q_o) = \nabla^2 T(\boldsymbol{x}, t; q_o), \quad (\boldsymbol{x}, t) \in \Omega_\ell(t) \times [0, t_{max}] \tag{2}$$

$$\frac{\partial c(\boldsymbol{x}, t; q_o)}{\partial t} + \boldsymbol{u}(\boldsymbol{x}, t; q_o) \cdot \nabla c(\boldsymbol{x}, t; q_o) = Le^{-1} \nabla^2 c(\boldsymbol{x}, t; q_o), \quad (\boldsymbol{x}, t) \in \Omega_\ell(t) \times [0, t_{max}] \tag{3}$$

$$\frac{\partial \boldsymbol{u}(\boldsymbol{x},t;q_o)}{\partial t}+\boldsymbol{u}(\boldsymbol{x},t;q_o)\cdot\nabla\boldsymbol{u}(\boldsymbol{x},t;q_o)=Pr\nabla^2\boldsymbol{u}(\boldsymbol{x},t;q_o)-Pr\,Ra_T T(\boldsymbol{x},t;q_o)\boldsymbol{e_g}$$
$$-Pr\,Ra_C\gamma c(\boldsymbol{x},t;q_o)\boldsymbol{e_g}-\nabla p(\boldsymbol{x},t;q_o),\quad (\boldsymbol{x},t)\in\Omega_\ell(t)\times[0,t_{max}] \tag{4}$$

$$\nabla\cdot\boldsymbol{u}(\boldsymbol{x},t;q_o)=0,\quad (\boldsymbol{x},t)\in\Omega_\ell(t)\times[0,t_{max}] \tag{5}$$

$$T(\boldsymbol{x},0)=1,\quad c(\boldsymbol{x},0)=0,\quad \boldsymbol{u}(\boldsymbol{x},0)=\boldsymbol{0},\quad \boldsymbol{x}\in\Omega_\ell(0) \tag{6}$$

$$\frac{\partial T}{\partial n}(\boldsymbol{x},t;q_o)=0,\quad (\boldsymbol{x},t)\in\Gamma_{h\ell}\times[0,t_{max}] \tag{7}$$

$$\frac{\partial T}{\partial n}(\boldsymbol{x},t;q_o)=q_{o\ell},\quad (\boldsymbol{x},t)\in\Gamma_{o\ell}\times[0,t_{max}] \tag{8}$$

$$\frac{\partial c}{\partial n}(\boldsymbol{x},t;q_o)=0,\quad (\boldsymbol{x},t)\in(\Gamma_{h\ell}\cup\Gamma_{o\ell})\times[0,t_{max}] \tag{9}$$

$$\boldsymbol{u}(\boldsymbol{x},t;q_o)=\boldsymbol{0},\quad (\boldsymbol{x},t)\in\Gamma_\ell\times[0,t_{max}] \tag{10}$$

$$\frac{\partial T(\boldsymbol{x},t;q_o)}{\partial t}=R_\alpha\nabla^2T(\boldsymbol{x},t;q_o),\quad (\boldsymbol{x},t)\in\Omega_s\times[0,t_{max}] \tag{11}$$

$$\frac{\partial T}{\partial n}(\boldsymbol{x},t;q_o)=q_{os},\quad (\boldsymbol{x},t)\in\Gamma_{os}\times[0,t_{max}] \tag{12}$$

$$\frac{\partial T}{\partial n}(\boldsymbol{x},t;q_o)=0,\quad (\boldsymbol{x},t)\in\Gamma_{hs}\times[0,t_{max}] \tag{13}$$

$$T(\boldsymbol{x},t;q_o)=c(\boldsymbol{x},t;q_o)\quad (\boldsymbol{x},t)\in\Gamma_I\times[0,t_{max}] \tag{14}$$

$$\frac{\partial c}{\partial n}(\boldsymbol{x},t;q_o)=Le[\boldsymbol{v}_f(\boldsymbol{x},t;q_o)\cdot\boldsymbol{n}](1-\kappa)[c(\boldsymbol{x},t;q_o)-\gamma^{-1}],\quad (\boldsymbol{x},t)\in\Gamma_I\times[0,t_{max}] \tag{15}$$

$$\frac{\partial T_l}{\partial n}(\boldsymbol{x},t;q_o)-R_k\frac{\partial T_s}{\partial n}(\boldsymbol{x},t;q_o)=Ste^{-1}\boldsymbol{v}_f(\boldsymbol{x},t;q_o)\cdot\boldsymbol{n},\quad (\boldsymbol{x},t)\in\Gamma_I\times[0,t_{max}], \tag{16}$$

where $R_\alpha=\alpha_s/\alpha_\ell$, $R_k=k_s/k_\ell$, $\boldsymbol{e_g}=\boldsymbol{g}/|\boldsymbol{g}|$ is the unit vector in the direction of gravity, and κ is defined in Fig. 2. The Stefan condition (Eq. (16)) can be used to define the interface motion. The thermodynamic equilibrium condition is stated with Eq. (14), which is derived from the dilute alloy phase diagram (Fig. 2).

Note that the above problem has been presented with q_o as a parameter. This emphasizes the parametric dependence of the solution $T(\boldsymbol{x},t)$, $c(\boldsymbol{x},t)$, $\boldsymbol{u}(\boldsymbol{x},t)$, and $\boldsymbol{v}_f(\boldsymbol{x},t)$ on the boundary heat fluxes $q_{o\ell}$ in Eq. (8) and q_{os} in Eq. (12). Finally, we note that for the reference direct problem of Fig. 1a, one must solve the above equation system, together with the a priori assumption of a stable sharp interface growth.

2.2. *A Reference Design Problem with a Desired Interface Growth*

Here we will introduce a reference design problem (see Fig. 1b) with $q_{ol}=0$ and a flat interface throughout the process of solidification. The inverse *reference design problem* is stated as follows: *Find the appropriate cooling heat flux $q_{os}(y,\ t)$ at the vertical solid mold wall Γ_{os} such that the solid/liquid freezing interface remains flat and advances with a spatially uniform velocity $\boldsymbol{v}_f(t)$ into the liquid.* The governing equations are still Eqs. (2)–(16), where the differences from the direct problem of Section 2.1 are that q_{os} in

Eq. (12) is problem unknown, while $\boldsymbol{v}_f$ in Eqs. (16) and (15) is explicitly given. Since the transient location of the interface $\Gamma_I(t)$ is given (through integration of $\boldsymbol{v}_f(t)$), the solid and liquid domains are known at all times. We can separate the above inverse problem into two subproblems and solve them sequentially:

- A quasi-direct problem in the liquid region $\Omega_\ell(t)$: Using Eqs. (2)–(10), (14), and (15), calculate the temperature, velocity, and concentration fields in the melt. The temperature and concentration gradients $G = \partial T_\ell/\partial n$ and $G_c = \partial c/\partial n$, respectively, at the interface Γ_I can be obtained from the temperature and concentration field solutions. In order to identify the present results with the reference problem of Fig. 1b, we will denote these calculated temperature and concentration gradients at the freezing front as G^{ref} and G_c^{ref}, respectively.
- An inverse heat conduction problem in the solid region $\Omega_s(t)$: Using Eq. (11) with the boundary condition Eq. (13) and the overspecifying boundary conditions on Γ_I (temperature and heat flux from the solution of the quasi-direct problem in the liquid and the Stefan condition from Eq. (16)), find the unknown heat flux $q_{os}(y, t)$ on Γ_{os}. Such a problem can be solved with the adjoint equation technique of [11] and it will not be repeated in this paper.

2.3. *Numerical Solution of the Reference Design Problem and a posteriori Examination of the Sharp Interface Assumption*

Let us take an example of the solidification of a NH_4Cl water solution (1.5% weight concentration) with initial overheating of $T_i - T_o = 20^\circ$C, in a rectangular cavity (dimensionless height $h = 1$, width $w = 0.5$), as shown in Fig. 1b. The inverse design objective is to realize a vertical flat interface moving from Γ_{os} to $\Gamma_{o\ell}$ at a constant dimensionless velocity $\boldsymbol{v}_f = 0.2$. The thermophysical properties are taken from [22] and are shown in Table 1. Solidification starts off at $t = 0^+$ when the $x = 0$ boundary is suddenly dropped to $T = 0$ (the dimensionless melting temperature at initial concentration) and runs up to $t_{max} = 1.5$ when 60% of the slab has solidified.

A moving finite element method is used to solve the system of Eqs. (2)–(10) (quasi-direct problem in the liquid melt). The initial mesh (at $t = 0$) used is shown in Fig. 3 and it contains 20×20 rectangular bilinear elements. The number of elements is maintained fixed at all times. These elements are deformed uniformly through out the process. The contribution of the mesh velocity is taken into account in the convective terms. A streamline upwind Petrov–Galerkin method is used, together with a predictor–corrector scheme for the

TABLE 1
Nondimensional Parameters Used for NH_4Cl–H_2O

Name/Meaning	Symbol	Definition	Value used
Prandtl number	Pr	$\frac{\nu}{\alpha_\ell}$	9.025
Lewis number	Le	$\frac{\alpha_\ell}{D\ell}$	27.845
Partition ratio	κ	c_s/c_ℓ on Γ_I	0.3
Relative initial overheat	γ	$(T_i - T_o)/(mc_o) + 1$	18.152
Thermal Rayleigh number	Ra_T	$[\lvert\boldsymbol{g}\rvert\beta_T(T_i - T_{ref})l^3]/(\nu\alpha_\ell)$	2.0×10^4
Solutal Rayleigh number	Ra_C	$[\lvert\boldsymbol{g}\rvert\beta_C c_o l^3]/(\nu\alpha_\ell)$	1.0×10^4

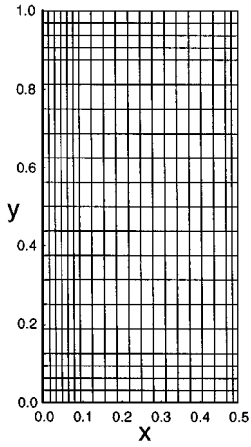

FIG. 3. The finite element mesh in the liquid melt at $t = 0$.

time integration of the discretized equations. The time step is taken as $\Delta t = 0.0004$ before $t = 0.02$ and $\Delta t = 0.004$ afterwards. The numerical implementation follows that of [23, 24], and it is similar to that presented in our earlier work [17].

From all the calculated results, we are particularly interested in the interface heat flux $G^{ref} \equiv G$ and concentration gradient $G_c^{ref} \equiv G_c$ (Figs. 4a and 4b, respectively). The calculated flux G, together with the calculated interface temperature can be used to solve the inverse conduction problem in the solid and obtain the heat flux $q_{os}(y, t)$. We will not present these results as we will next show that the calculated G^{ref} and G_c^{ref} are already in contradiction with the assumption of a stable sharp interface between the two phases.

The absence of constitutional undercooling in the liquid melt is used here as a simplified form of the necessary conditions for interface stability. This condition is expressed mathematically as

$$G < G_c, \tag{17}$$

where $G = \partial T/\partial n$ and $G_c = \partial c/\partial n$ are the gradients in the normal direction of the dimensionless temperature and concentration fields at the liquid side of the interface, respectively. Note that the above equation can also be written in a more familiar form as in [19], $G > mG_c$, where G and G_c are the magnitudes of the gradients of the dimensional temperature and concentration fields at the liquid side of the solid–liquid interface and m is the magnitude of the slope of the liquidus line in the phase diagram (Fig. 2). Equation (17) is here written in a nondimensional form and using a normal unit vector $\boldsymbol{n}$ at the interface boundary that points towards the solid phase.

The solution of the reference design problem given in Figs. 4a, b does not satisfy Eq. (17). Indeed, let us examine if the solution is such that $\Delta G = G - G_c < 0$ is satisfied. From Fig. 4c (the earlier stage $\Delta G < -1.0$ is not shown) we do observe that $\Delta G > 0$ some time after solidification started. The stability condition is only satisfied at the early stages of solidification (the shaded region of Fig. 4d). At later times, constitutional undercooling has occurred in the liquid. The physical explanation for the onset of such undercooling mainly lies in the difference between the thermal and solutal diffusivities (their ratio $Le \gg 1$) and because the rejected solute at the interface cannot be diffused as fast as the heat.

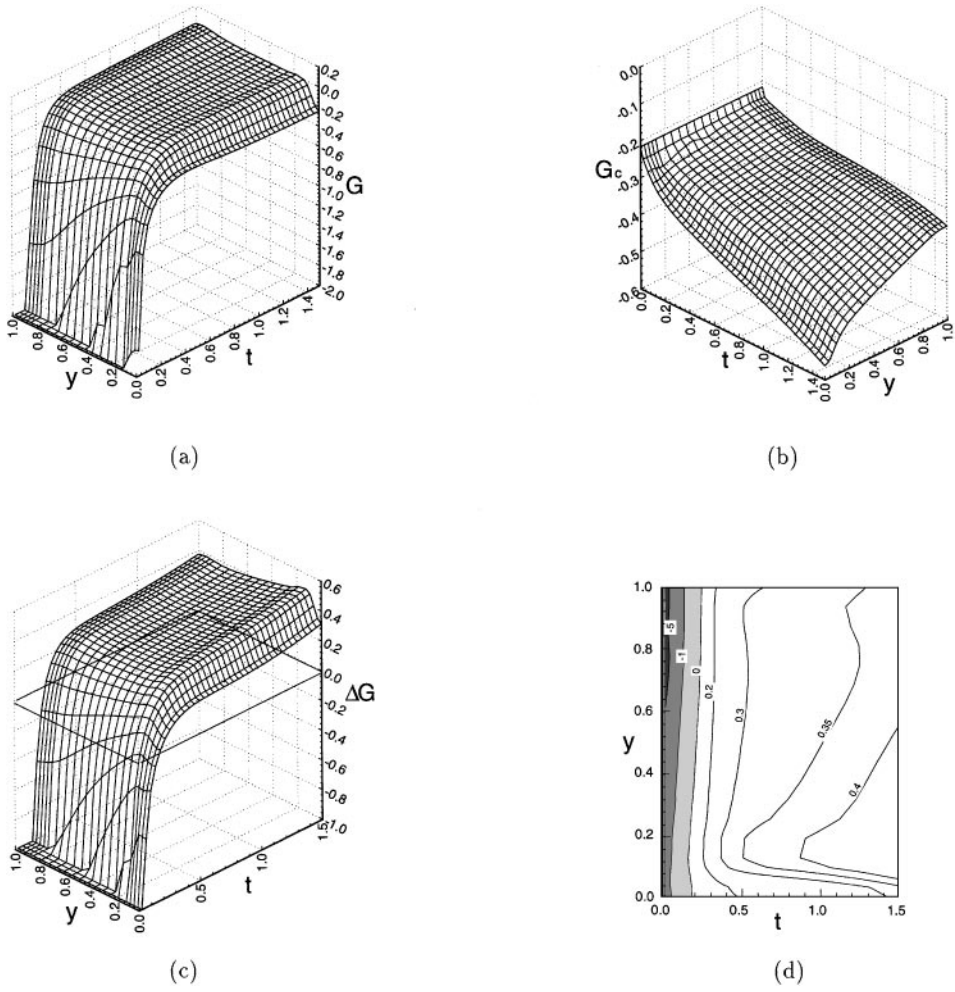

FIG. 4. Examination of the constitutional stability assumption at the solid–liquid interface for the reference design problem: (a) interface temperature gradient $G^{ref}(y,t) = (\partial T/\partial n)(v_f t, y; t)$; (b) interface concentration gradient $G_c^{ref}(y,t) = (\partial c/\partial n)(v_f t, y; t)$; (c) difference $\Delta G^{ref} = G^{ref} - G_c^{ref}$; (d) contour lines of ΔG^{ref} in the (y,t) plane.

The above mathematical model with the assumption of a sharp solid/liquid interface is thus not physically realistic.

3. INVERSE DESIGN TO ACHIEVE A DESIRED STABLE GROWTH

Referring to the reference design problem of Section 2.2 and in order to achieve a desired interface growth, we relax the adiabatic condition q_{ol} at the mold wall $\Gamma_{o\ell}$ in the reference problem of Fig. 1. With a similar configuration, we pose using Fig. 5a the following inverse design problem: *Find the cooling condition at* Γ_{os} *as well as the heat flux condition* $q_{o\ell}(y,t)$ *at the vertical mold wall* $\Gamma_{o\ell}$, *in order to achieve a desired growth of the interface* (*the same as that in the reference problem of Fig.* 1b) *that is ensured to be constitutionally stable* (*i.e., Eq.* (17) *is satisfied*).

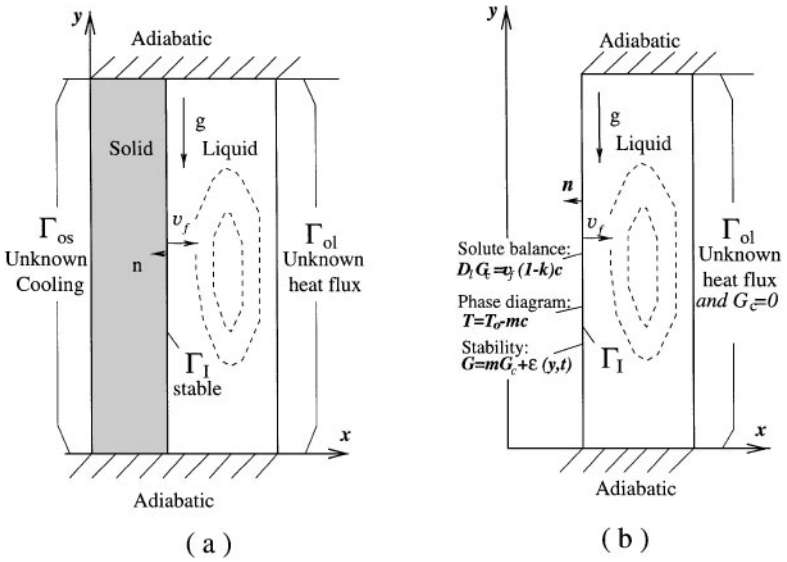

FIG. 5. Schematic of the inverse problem to achieve a sharp interface moving with a desired growth velocity $\mathbf{v}_f$ during solidification of a binary alloy in a rectangular cavity: (a) problem requirement and unknowns; (b) inverse subproblem in the liquid phase.

Such an inverse problem can be separated into two subproblems, one inverse problem in the solid and another inverse problem in the liquid region, respectively. This is possible since, as part of the design objectives, we consider that the location of the interface Γ_I is explicitly given through the growth velocity $\boldsymbol{v}_f(t)$. The inverse problem in the solid is an inverse heat conduction problem. The inverse problem in the liquid, as shown in Fig. 5b, is to find the unknown heat flux $q_{o\ell}(y, t)$ at the vertical liquid mold wall $\Gamma_{o\ell}$, such that at the liquid side of the interface Γ_I the following conditions are satisfied: the solute balance (Eq. (15)), the phase diagram liquidus relation (Eq. (14)), and the constitutional stability condition (Eq. (17)). This is a typical inverse problem with overspecified boundary conditions. In this problem, three boundary conditions are given at the interface Γ_I relating the temperature T and the concentration c. We also have the solute impermeable condition equation (9) and an unknown thermal flux condition at the mold wall $\Gamma_{o\ell}$. The major objective of this paper is to solve such an inverse problem involving heat and solute transport and thermo-solutal convective flow. We call such an inverse design problem with coupled heat, mass, and flow transport mechanisms, *an inverse design thermo-solutal convection problem*. To our knowledge, this is the first time that a *continuum formulation* is proposed for the solution of inverse problems for such coupled continuum systems.

3.1. *Enforcement of the Constitutional Stability Condition*

Notice that the stability requirement of Eq. (17) is in an inequality form. We can transform it to the nondimensional equality form

$$\frac{\partial T}{\partial n} = \frac{\partial c}{\partial n} + \epsilon(y, t), \tag{18}$$

where $\epsilon \leq 0$. The specific form of ϵ is part of the inverse problem definition. However, there is freedom in the selection of any nonpositive $\epsilon(y, t)$ in order to enforce stability. Let

us recall the time variation of ΔG in the reference example of the last section (ΔG^{ref}) and the loss of stability when $\Gamma_{o\ell}$ was simply kept adiabatic. We will here use the calculated $\Delta G^{ref}(y, t)$ in the reference design problem (Fig. 4c) as a basis for choosing ϵ and make the necessary adjustments to ϵ when ΔG becomes positive (i.e., when the interface of the reference design becomes unstable). In particular, we select the form of the stability condition,

$$\Delta G(y,t) \equiv \epsilon(y,t) = \begin{cases} \Delta G^{ref}(y,t), & \text{if } \Delta G^{ref}(y,t) < \delta Le\gamma^{-1}(1-\kappa)(\boldsymbol{v}_f(t)\cdot\boldsymbol{n}), \\ \delta Le\gamma^{-1}(1-\kappa)(\boldsymbol{v}_f(t)\cdot\boldsymbol{n}), & \text{if } \Delta G^{ref}(y,t) \geq \delta Le\gamma^{-1}(1-\kappa)(\boldsymbol{v}_f(t)\cdot\boldsymbol{n}), \end{cases} \tag{19}$$

where δ is chosen as a small scalar parameter. Also, recall that due to the selection of the direction of $\boldsymbol{n}$, $\boldsymbol{v}_f(t)\cdot\boldsymbol{n} < 0$. As $\delta \to 0$, $\epsilon \to 0$ which means that marginal stability is maintained after $\Delta G^{ref} > 0$. The underlying physics for such a choice is to pursue minimum heating flux input at the liquid boundary mold wall $\Gamma_{o\ell}$, thus minimum cooling at the solid mold wall Γ_{os} and overall a minimum energy consumption that ensures the desired stable growth. The "over-stable" amount parameterized by δ is introduced for numerical accuracy considerations since, theoretically, the optimum heat flux $q_{o\ell}(y, t)$ at $\Gamma_{o\ell}$ calculated with $\epsilon = 0$ may also be able to avoid the occurrence of $\Delta G > 0$. However, the design for an interface that is slightly over-stable will compensate for the numerical error in the implementation of the discretized problem. The specific form of such an over-stable amount can be understood from its equivalent dimensional form,

$$G = m\left[G_c + \delta\frac{c_o}{D_\ell}(1-\kappa)|\boldsymbol{v}_f(t)\cdot\boldsymbol{n}|\right], \tag{20}$$

where, following the notation of [19], G and G_c are in the above equation referring to the magnitudes of the corresponding gradients of T and c, respectively. The second term on the right hand side of the above equation can be thought of as the perturbation of G_c by a δ portion of its estimation through the dimensional form of Eq. (15) with a fixed $c = c_o$ on the right-hand side of Eq. (15).

There might be physical considerations other than marginal stability/minimum energy consumption that someone can use to choose $\epsilon(y, t)$, such as minimization of the solute inhomogeneity in the final solidified product. Since this paper represents the first study of the inverse design of stable interface growth, we will only use the simplified marginal stability conditions given here with ϵ based on Eq. (19).

3.2. *The Adjoint Method Formulation*

3.2.1. Definition of the optimization problem. The inverse design thermo-solutal convection problem in the liquid can be formulated as an optimization problem. With the *guessed* heat flux condition at the liquid boundary mold wall,

$$\frac{\partial T}{\partial n}(\boldsymbol{x}, t) = q_{o\ell}(\boldsymbol{x}, t), \quad (\boldsymbol{x}, t) \in \Gamma_{o\ell} \times [0, t_{max}], \tag{21}$$

and using Eqs. (2)–(5), initial conditions equation (6), and boundary conditions equations (7)–(10) and (18), one can define a direct thermal-solutal convection problem on a prescribed domain $\Omega_\ell(t)$. Let us denote its solution for the temperature, concentration, and

flow fields as $T(\boldsymbol{x}, t; q_{o\ell})$, $c(\boldsymbol{x}, t; q_{o\ell})$, and $\boldsymbol{u}(\boldsymbol{x}, t; q_{o\ell})$, respectively, indicating their parametric dependence on $q_{o\ell}$. Note that the liquidus relation equation (14) is not used in this *direct problem* definition, thus it is not certain that it will be satisfied. Instead, for arbitrary $q_{o\ell} \in L_2(\Gamma_{o\ell} \times [0, t_{max}])$ we define a cost functional

$$S(q_{o\ell}) = \int_0^{t_{max}} \int_{\Gamma_I} [T(\boldsymbol{x}, t; q_{o\ell}) - c(\boldsymbol{x}, t; q_{o\ell})]^2 \, d\Gamma \, dt \tag{22}$$

to indicate the discrepancy of the calculated temperature from the concentration-dependent liquidus temperature at the interface. In the most familiar dimensional form, the above cost functional is defined using the discrepancy between the calculated interface temperature T and the equilibrium freezing temperatute $(T_o - mc)$. Such a cost functional can be thought of as a measure of the deviation of the interface from the thermal conditions corresponding to thermodynamic equilibrium.

The inverse problem in the liquid is restated in a minimization sense as follows: *Find a quasi-solution* $\hat{q}_{o\ell} \in L_2(\Gamma_{o\ell} \times [0, t_{max}])$ *such that*

$$S(\hat{q}_{o\ell}) \leq S(q_{o\ell}) \quad \forall \, q_{o\ell} \in L_2(\Gamma_{o\ell} \times [0, t_{max}]),$$

where T and c in the functional S are defined by Eqs. (2)–(5), (6), (7)–(10) and Eq. (18) for a given $q_{o\ell}$.

Certain compatibility conditions are generally required between the given data $\boldsymbol{v}_f$, ϵ, the material properties, and geometry in order for a solution of the inverse problem to exist with $S(\hat{q}_{o\ell}) = 0$. In this paper, our objective is to construct a minimizing sequence $q^i_{o\ell}(\boldsymbol{x}, t) \in L_2(\Gamma_{o\ell} \times [0, t_{max}])$, $i = 1, 2, \ldots$, that converges to at least a local minimum of $S(q_{o\ell})$. If such a minimum can lead to an interface growth that is close enough to the desired growth conditions and is constitutionally stable, then an acceptable design solution has been obtained.

3.2.2. *Governing equations of the sensitivity problem.* To perform the optimization procedure that minimizes $S(q_{o\ell})$ in $L_2(\Gamma_o \times [0, t_{max}])$, we will need to define a *continuum sensitivity problem*. This linear problem defines the linear perturbations $\Theta(\boldsymbol{x}, t; q_{o\ell}, \Delta q_{o\ell}) \equiv D_{\Delta q_{o\ell}} T(\boldsymbol{x}, t; q_{o\ell})$, $C(\boldsymbol{x}, t; q_{o\ell}, \Delta q_{o\ell}) \equiv D_{\Delta q_{o\ell}} c(\boldsymbol{x}, t; q_{o\ell})$, and $\boldsymbol{U}(\boldsymbol{x}, t; q_{o\ell}, \Delta q_{o\ell}) \equiv D_{\Delta q_{o\ell}} \boldsymbol{u}(\boldsymbol{x}, t; q_{o\ell})$ of the fields $T(\boldsymbol{x}, t; q_{o\ell})$, $c(\boldsymbol{x}, t; q_{o\ell})$, and $\boldsymbol{u}(\boldsymbol{x}, y; q_{o\ell})$, respectively, due to variations $\Delta q_{o\ell}(\boldsymbol{x}, t)$ of the boundary heat flux $q_{o\ell}$, i.e.,

$$T(\boldsymbol{x}, t; q_{o\ell} + \Delta q_{o\ell}) = T(\boldsymbol{x}, t; q_{o\ell}) + \Theta(\boldsymbol{x}, t; q_{o\ell}, \Delta q_{o\ell}) + O\left(\|\Delta q_{o\ell}\|^2_{L_2(\Gamma_{o\ell} \times [0, t_{max}])}\right) \tag{23}$$

$$c(\boldsymbol{x}, t; q_{o\ell} + \Delta q_{o\ell}) = c(\boldsymbol{x}, t; q_{o\ell}) + C(\boldsymbol{x}, t; q_{o\ell}, \Delta q_{o\ell}) + O\left(\|\Delta q_{o\ell}\|^2_{L_2(\Gamma_{o\ell} \times [0, t_{max}])}\right) \tag{24}$$

$$\boldsymbol{u}(\boldsymbol{x}, t; q_{o\ell} + \Delta q_{o\ell}) = \boldsymbol{u}(\boldsymbol{x}, t; q_{o\ell}) + \boldsymbol{U}(\boldsymbol{x}, t; q_{o\ell}, \Delta q_{o\ell}) + O\left(\|\Delta q_{o\ell}\|^2_{L_2(\Gamma_{o\ell} \times [0, t_{max}])}\right). \tag{25}$$

Linearization of the direct problem results in the continuum *sensitivity problem*

$$\frac{\partial \Theta(\boldsymbol{x}, t; q_o, \Delta q_o)}{\partial t} + \boldsymbol{u}(\boldsymbol{x}, t; q_o, \Delta q_o) \cdot \nabla \Theta(\boldsymbol{x}, t; q_o, \Delta q_o) + \boldsymbol{U}(\boldsymbol{x}, t; q_o, \Delta q_o) \cdot \nabla T(\boldsymbol{x}, t; q_o)$$
$$= \nabla^2 \Theta(\boldsymbol{x}, t; q_o, \Delta q_o), \quad (\boldsymbol{x}, t) \in \Omega_\ell(t) \times [0, t_{max}] \tag{26}$$

$$\frac{\partial C(\boldsymbol{x}, t; q_o, \Delta q_o)}{\partial t} + \boldsymbol{u}(\boldsymbol{x}, t; q_o, \Delta q_o) \cdot \nabla C(\boldsymbol{x}, t; q_o, \Delta q_o) + \boldsymbol{U}(\boldsymbol{x}, t; q_o, \Delta q_o) \cdot \nabla c(\boldsymbol{x}, t; q_o)$$
$$= Le^{-1} \nabla^2 C(\boldsymbol{x}, t; q_o, \Delta q_o), \quad (\boldsymbol{x}, t) \in \Omega_\ell(t) \times [0, t_{max}] \tag{27}$$

$$\frac{\partial \boldsymbol{U}(\boldsymbol{x}, t; q_o, \Delta q_o)}{\partial t} + \boldsymbol{u}(\boldsymbol{x}, t; q_o) \cdot \nabla \boldsymbol{U}(\boldsymbol{x}, t; q_o, \Delta q_o) + \boldsymbol{U}(\boldsymbol{x}, t; q_o, \Delta q_o) \cdot \nabla \boldsymbol{u}(\boldsymbol{x}, t; q_o)$$
$$= -\nabla \cdot \Pi(\boldsymbol{x}, t; q_o) + Pr \nabla^2 \boldsymbol{U}(\boldsymbol{x}, t; q_o, \Delta q_o) - Pr\, Ra_T \Theta(\boldsymbol{x}, t; q_o, \Delta q_o) \boldsymbol{e_g}$$
$$+ \gamma Ra_C C(\boldsymbol{x}, t; q_o, \Delta q_o) \boldsymbol{e_g}, \quad (\boldsymbol{x}, t) \in \Omega_\ell(t) \times [0, t_{max}], \tag{28}$$

$$\nabla \cdot \boldsymbol{U}(\boldsymbol{x}, t; q_o, \Delta q_o) = 0, \quad (\boldsymbol{x}, t) \in \Omega_\ell(t) \times [0, t_{max}], \tag{29}$$

$$\Theta(\boldsymbol{x}, 0; q_o, \Delta q_o) = 0, \quad \boldsymbol{x} \in \Omega_\ell(0), \tag{30}$$

$$C(\boldsymbol{x}, 0; q_o, \Delta q_o) = 0, \quad \boldsymbol{x} \in \Omega_\ell(0), \tag{31}$$

$$\boldsymbol{U}(\boldsymbol{x}, 0; q_o, \Delta q_o) = \boldsymbol{0}, \quad \boldsymbol{x} \in \Omega_\ell(0), \tag{32}$$

$$\frac{\partial \Theta}{\partial n}(\boldsymbol{x}, t; q_o, \Delta q_o) = 0, \quad (\boldsymbol{x}, t) \in (\Gamma_{h\ell} \cup \Gamma_I) \times [0, t_{max}], \tag{33}$$

$$\frac{\partial \Theta}{\partial n}(\boldsymbol{x}, t; q_o, \Delta q_o) = \Delta q_o(\boldsymbol{x}, t), \quad (\boldsymbol{x}, t) \in \Gamma_{o\ell} \times [0, t_{max}], \tag{34}$$

$$\frac{\partial C}{\partial n}(\boldsymbol{x}, t; q_o, \Delta q_o) = 0, \quad (\boldsymbol{x}, t) \in (\Gamma_{h\ell} \cup \Gamma_{o\ell}) \times [0, t_{max}], \tag{35}$$

$$\frac{\partial C}{\partial n}(\boldsymbol{x}, t; q_o, \Delta q_o) = Le(1 - \kappa)(\boldsymbol{v}_f \cdot \boldsymbol{n}) C(\boldsymbol{x}, t; q_o, \Delta q_o), \quad (\boldsymbol{x}, t) \in \Gamma_I \times [0, t_{max}], \tag{36}$$

$$\boldsymbol{U}(\boldsymbol{x}, t; q_o, \Delta q_o) = \boldsymbol{0}, \quad (\boldsymbol{x}, t) \in \Gamma_\ell \times [0, t_{max}], \tag{37}$$

where Π is the sensitivity pressure.

3.2.3. *Governing equations of the adjoint problem.* In order to realize the minimization of $S(q_{o\ell})$, it is essential to find its gradient (derivative) $S'(q_{o\ell})$ with respect to $q_{o\ell}$ that is defined by:

$$D_{\Delta q_{o\ell}} S(q_{o\ell}) = \int_0^{t_{max}} \int_{\Gamma_{o\ell}} S'(q_{o\ell}(\boldsymbol{x}, t)) \Delta q_{o\ell}(\boldsymbol{x}, t)\, d\Gamma\, dt. \tag{38}$$

After some lengthy manipulations (see [25]), we can define the *adjoint problem*

$$\frac{\partial \psi(\boldsymbol{x}, t; q_o)}{\partial t} + \boldsymbol{u}(\boldsymbol{x}, t; q_o) \cdot \nabla \psi(\boldsymbol{x}, t; q_o) = -\nabla^2 \psi(\boldsymbol{x}, t; q_o) + \phi(\boldsymbol{x}, t; q_o) \cdot \boldsymbol{e_g},$$
$$(\boldsymbol{x}, t) \in \Omega_\ell(t) \times [0, t_{max}], \tag{39}$$

$$\frac{\partial \varphi(\boldsymbol{x}, t; q_o)}{\partial t} + \boldsymbol{u}(\boldsymbol{x}, t; q_o) \cdot \nabla \varphi(\boldsymbol{x}, t; q_o) = -Le^{-1} \left[\nabla^2 \varphi(\boldsymbol{x}, t; q_o) + \frac{\gamma Ra_C}{Ra_T} \phi(\boldsymbol{x}, t; q_o) \cdot \boldsymbol{e_g} \right],$$
$$(\boldsymbol{x}, t) \in \Omega_\ell(t) \times [0, t_{max}], \tag{40}$$

$$\frac{\partial \phi(\boldsymbol{x}, t; q_o)}{\partial t} + \boldsymbol{u}(\boldsymbol{x}, t; q_o) \cdot \nabla \phi(\boldsymbol{x}, t; q_o) - [\nabla \boldsymbol{u}(\boldsymbol{x}, t; q_o)]^T \phi(\boldsymbol{x}, t; q_o)$$
$$= -Pr \nabla^2 \phi(\boldsymbol{x}, t; q_o) - \nabla \pi(\boldsymbol{x}, t; q_o) + Pr\, Ra_T [\psi(\boldsymbol{x}, t; q_o) \nabla T(\boldsymbol{x}, t; q_o)$$
$$- Le \varphi(\boldsymbol{x}, t; q_o) \nabla c(\boldsymbol{x}, t; q_o)], \quad (\boldsymbol{x}, t) \in \Omega_\ell(t) \times [0, t_{max}], \tag{41}$$

$$\nabla \cdot \boldsymbol{\phi}(\boldsymbol{x}, t; q_o) = 0, \quad (\boldsymbol{x}, t) \in \Omega_\ell(t) \times [0, t_{max}], \tag{42}$$

with end conditions

$$\begin{aligned} \psi(\boldsymbol{x}, t_{max}; q_o) &= \varphi(\boldsymbol{x}, t_{max}; q_o) = 0, \quad \boldsymbol{x} \in \Omega_\ell(t_{max}), \\ \boldsymbol{\phi}(\boldsymbol{x}, t_{max}; q_o) &= \mathbf{0}, \quad \boldsymbol{x} \in \Omega_\ell(t_{max}), \end{aligned} \tag{43}$$

and the boundary conditions

$$\frac{\partial \psi(\boldsymbol{x}, t; q_o)}{\partial n} - (\boldsymbol{v}_f \cdot \boldsymbol{n})\psi(\boldsymbol{x}, t; q_o) = T(\boldsymbol{x}, t; q_o) - c(\boldsymbol{x}, t; q_o), \quad (\boldsymbol{x}, t) \in \Gamma_I \times [0, t_{max}], \tag{44}$$

$$\frac{\partial \varphi(\boldsymbol{x}, t; q_o)}{\partial n} = Le(\boldsymbol{v}_f \cdot \boldsymbol{n})[\kappa\varphi(\boldsymbol{x}, t; q_o) + (1-\kappa)\psi(\boldsymbol{x}, t; q_o)] + T(\boldsymbol{x}, t; q_o) - c(\boldsymbol{x}, t; q_o), \quad (\boldsymbol{x}, t) \in \Gamma_I \times [0, t_{max}], \tag{45}$$

$$\frac{\partial \psi(\boldsymbol{x}, t; q_o)}{\partial n} = 0, \quad (\boldsymbol{x}, t) \in (\Gamma_{o\ell} \cup \Gamma_{h\ell}) \times [0, t_{max}], \tag{46}$$

$$\frac{\partial \varphi(\boldsymbol{x}, t; q_o)}{\partial n} = 0, \quad (\boldsymbol{x}, t) \in (\Gamma_{o\ell} \cup \Gamma_{h\ell}) \times [0, t_{max}], \tag{47}$$

$$\boldsymbol{\phi}(\boldsymbol{x}, t; q_o) = \mathbf{0}, \quad (\boldsymbol{x}, t) \in \Gamma_\ell \times [0, t_{max}]. \tag{48}$$

It can be shown that the gradient of $S(q_{o\ell})$ is given as [25]

$$S'(q_{o\ell}) = \psi(\boldsymbol{x}, t; q_{o\ell}), \quad (\boldsymbol{x}, t) \in \Gamma_{o\ell} \times [0, t_{max}]. \tag{49}$$

In the limit case of $Le \to 0$, the adjoint equations for $(\psi, \boldsymbol{\phi})$ are decoupled from those for φ. The adjoint system is reduced to an identical form to that developed earlier for inverse natural convection problems [17, 18].

3.2.4. *The conjugate gradient algorithm.* We have outlined above the definition of the continuous direct, adjoint, and sensitivity problems. The conjugate gradient method (CGM) can now be used for the minimization of the cost functional $S(q_{o\ell})$. It constructs a sequence: $q^0_{o\ell}, q^1_{o\ell}, \ldots, q^i_{o\ell}, \ldots$, to approach the optimal minimizer $\hat{q}_{o\ell}$ [26, 27]. The optimization procedure is the following:

Step A. Make an initial guess of $q^0_{o\ell}(\boldsymbol{x}, t) \in L_2(\Gamma_{o\ell} \times [0, t_{max}])$ and set $i = 0$.

Step B. Calculate the conjugate search direction $p^i(\boldsymbol{x}, t)$, $(\boldsymbol{x}, t) \in \Gamma_{o\ell} \times [0, t_{max}]$:

1. Solve the direct problem for $T(\boldsymbol{x}, t; q^i_{o\ell})$, $c(\boldsymbol{x}, t; q^i_{o\ell})$, and $\boldsymbol{u}(\boldsymbol{x}, t; q^i_{o\ell})$.
2. Compute the residual $[T(\boldsymbol{x}, t; q^i_{o\ell}) - c(\boldsymbol{x}, t; q^i_{o\ell})]$ for $(\boldsymbol{x}, t) \in \Gamma_I \times [0, t_{max}]$.
3. Evaluate $S(q^i_{o\ell})$ from Eq. (22); If $S(q^i_{o\ell}) < tol$ (given tolerance), set $\hat{q}_{o\ell} = q^i_{o\ell}$ and stop.
4. Solve the adjoint problem backwards in time for $\psi(\boldsymbol{x}, t; q^i_{o\ell})$.
5. Set $S'(q^i_{o\ell}) = \psi(\boldsymbol{x}, t; q^i_{o\ell})$ for $(\boldsymbol{x}, t) \in \Gamma_{o\ell} \times [0, t_{max}]$.
6. Set $\gamma^i = 0$, if $i = 0$; otherwise,

$$\gamma^i = \frac{\left(S'\left(q^i_{o\ell}\right), S'\left(q^i_{o\ell}\right) - S'\left(q^{i-1}_{o\ell}\right)\right)_{L_2(\Gamma_{o\ell} \times [0, t_{max}])}}{\left\| S'\left(q^{i-1}_{o\ell}\right) \right\|^2_{L_2(\Gamma_{o\ell} \times [0, t_{max}])}}.$$

7. Define $p^i(\boldsymbol{x}, t)$. If $i = 0$ set $p^0 = -S'(q^i_o)$; otherwise, $p^i = -S'(q^i_o)(\boldsymbol{x}, t) + \gamma^i p^{i-1}$.

Step C. Calculate the optimal step size α^i:

1. Solve the sensitivity problem for $\Theta(\boldsymbol{x}, t; q^i_{o\ell}, p^i)$, $C(\boldsymbol{x}, t; q^i_{o\ell}, p^i)$, and $\boldsymbol{U}(\boldsymbol{x}, t; q^i_{o\ell}, p^i)$.

2. Calculate α^i by

$$\alpha^i = \frac{-\left(S'(q^i_{o\ell}), p^i\right)_{L_2(\Gamma_{o\ell}\times[0,t_{max}])}}{\left\|\Theta(\boldsymbol{x}, t; q^i_{o\ell}, p^i) - C(\boldsymbol{x}, t; q^i_{o\ell}, p^i)\right\|^2_{L_2(\Gamma_I\times[0,t_{max}])}}.$$

Step D. Update $q^{i+1}_{o\ell}(\boldsymbol{x}, t) = q^i_{o\ell}(\boldsymbol{x}, t) + \alpha^i p^i(\boldsymbol{x}, t)$, $(\boldsymbol{x}, t) \in \Gamma_{o\ell} \times [0, t_{max}]$.

Step E. Set $i = i + 1$ and go to Step B.

The inner product in the L_2 space involved in the CGM procedure is defined as

$$(f, g)_{L_2(\Gamma\times[0,t_{max}])} = \int_0^{t_{max}} \int_\Gamma fg \, d\Gamma \, dt. \tag{50}$$

4. NUMERICAL IMPLEMENTATION, RESULTS, AND DISCUSSION

The inverse algorithm of Section 3 is implemented here for the solidification of NH_4Cl–H_2O that was also used in the reference design problem of Section 2.3. However, the objective here is to find the transient histories of heat fluxes at $x = 0.5$ and at $x = 0$ that result in a stable growth with a desired constant front velocity. To overcome the difficulty of the end condition of the adjoint method (recall that based on Eq. (43) and for each iteration i we have that, $q^i_{o\ell}(y, t_{max}) = q^0_{o\ell}(y, t_{max})$; i.e., $q^i_{o\ell}(y, t_{max})$ maintains its value from the initial guess solution), we modify the choice of the interface growth velocity as follows:

$$\boldsymbol{v}_f(t) = \begin{cases} v_o, & 0 \le t \le t_{mid}, \\ v_o \frac{t_{max}-t}{t_{max}-t_{mid}}, & t_{mid} < t < t_{max}. \end{cases} \tag{51}$$

Integration of $\boldsymbol{v}_f(t)$ gives the resultant desired interface location as

$$s(t) = \begin{cases} v_o t, & 0 \le t \le t_{mid}, \\ \frac{v_o}{2}\left[t_{mid} + t_{max} - \frac{(t_{max}-t)^2}{(t_{max}-t_{mid})}\right], & t_{mid} < t < t_{max}, \end{cases} \tag{52}$$

where we select the dimensionless parameters as $v_o = 0.2$, $t_{mid} = 1.5$, and $t_{max} = 2.0$. An initial guess $q^0_{o\ell}(y, t) = 0$ is made. The desired interface growth slows down after $t = t_{mid}$ and is such that $\boldsymbol{v}_f(t_{max}) = 0$. The selection of $\boldsymbol{v}_f$ $(t > t_{mid}) \to 0$ allows the interface concentration gradient $G_c \to 0$ and leads to a solutal convection that dies out for $t > t_{mid}$. The thermal field is also expected to be smoothed out by time t_{max} and thus the approximation $q_{o\ell}(y, t_{max}) = 0$ is a reasonable one.

The finite element formulation is similar to that presented in our previous work [17, 18]. The time stepping technique for the direct and sensitivity problems is a semi-implicit predictor/corrector procedure [23], while a Crank–Nicholson scheme is used for the time discretization of the adjoint problem. The adjoint problem is linear, including the coupling among adjoint thermal, concentration, and velocity equations, and thus no

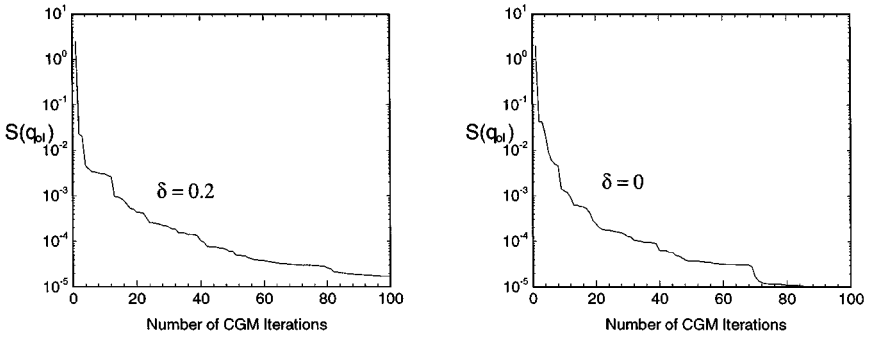

FIG. 6. Convergence of the cost functional $S(q_{o\ell})$ for $\delta = 0.2$ and $\delta = 0$ (note that the $\delta = 0.2$ case converges slightly slower).

Newton–Raphson type of iterations are needed within a time step for its solution. The same time step is used for the direct, sensitivity, and adjoint problems. This is important considering that the solution of the adjoint problem requires the solution of the direct problem at all time levels. The discretized equations are similar to those in [17].

The finite element mesh and time step sizes are the same as those used for the solution of the reference problem in Section 2.3. The total number of time steps is 545 for each of the direct, adjoint, and sensitivity problems in a single CGM iteration. The cost of each CGM iteration was about 1 h CPU time on the IBM/RS6000 (SP2). As a preliminary study of the solution of such inverse problems and in consideration of the computational cost, the Rayleigh number used here (see Table 1) is lower than the actual number under normal laboratory conditions.

For purposes of performing an accuracy study and comparison, both $\delta = 0$ and $\delta = 0.2$ are chosen as the parameter for "over stability" in Eq. (19). The $\delta = 0$ case is seeking a heat flux solution that strictly leads to marginal stability. For this case, the CGM algorithm proceeds up to 100 iterations when the cost functional $S \sim O(10^{-5})$, as shown in Fig. 6. Final optimum heat flux solutions $\hat{q}_{o\ell}(y, t)$ are shown in Fig. 7. The calculated flux $q^k_{o\ell}(y, t)$ at various CGM iterations is also shown in Fig. 8.

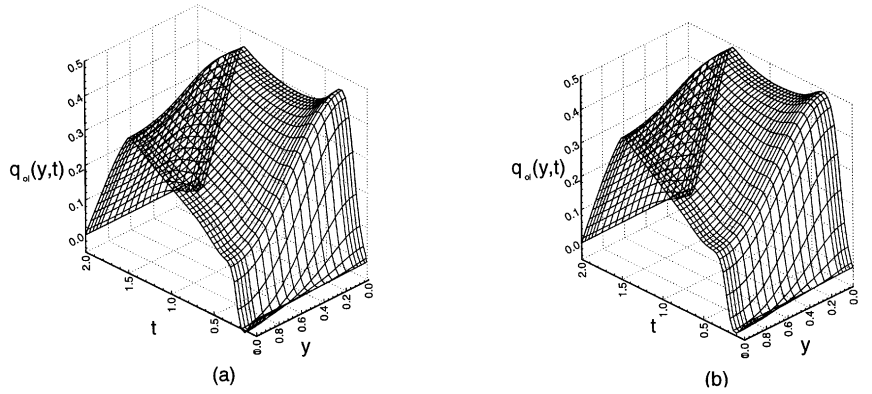

FIG. 7. Optimum heat flux $\hat{q}_{o\ell}(y, t)$ for (a) $\delta = 0$ and (b) $\delta = 0.2$. Both results correspond to heating except at the very early stages of solidification.

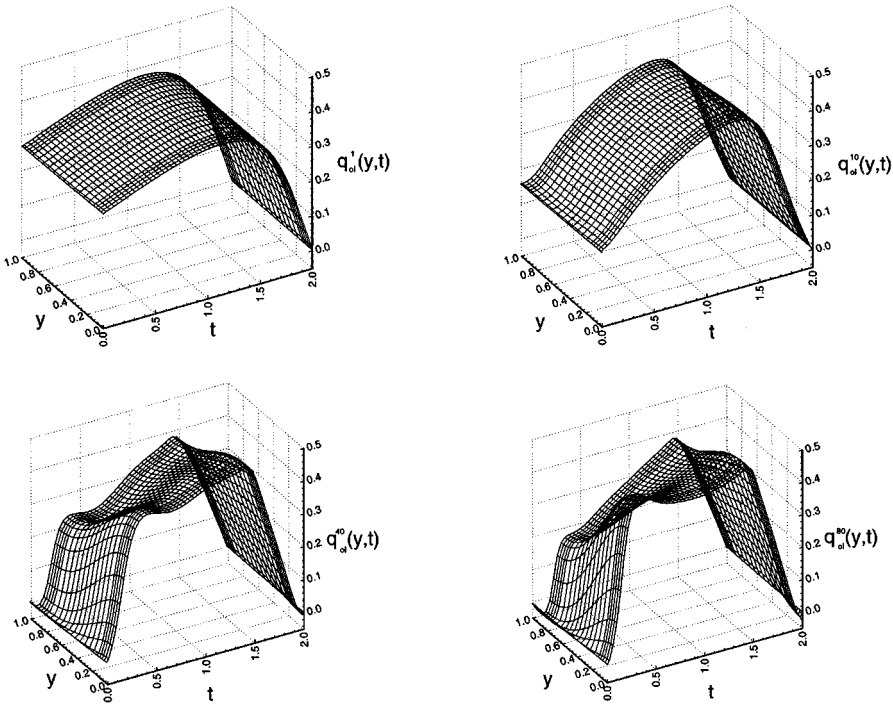

FIG. 8. $q^i_{ol}(y, t)$ at the intermediate $i = 1$, 10, 40, and 80 iterations ($\delta = 0.2$). The temporal features of $q_{o\ell}$ are reconstructed at early iterations, whereas accurate reconstruction of the spatial variations requires more iterations.

For the final optimum heat flux, we define the following quantity indicating the energy input into the melt at the mold wall $\Gamma_{o\ell}$:

$$Q = \int_0^{t_{max}} \int_0^1 \hat{q}_{o\ell}(y, t) dy\, dt. \tag{53}$$

Since $\hat{q}_{o\ell}$ is the solution corresponding to the parameter δ, Q will also depend on δ. In this example, $Q|_{\delta=0} = 0.5173$ and $Q|_{\delta=0.2} = 0.5828$. Their difference is very close to $\int_0^{tmax} \int_0^1 (\epsilon|_{\delta=0} - \epsilon|_{\delta=0.2}) dy dt = 0.066$, which is consistent with an energy balance. The amount of heat input required at the mold wall boundary is directly related to the amount of "over stability" imposed or achieved at the freezing interface.

A validation procedure is performed to check the accuracy of the interface stability about the optimum heat flux solution $\hat{q}_{o\ell}(y, t)$. A quasi-direct problem in the liquid as in Section 2.2 is solved, using the obtained $\hat{q}_{o\ell}(y, t)$ as boundary condition at the $\Gamma_{o\ell}$ mold wall at $x = 0.5$. Using an approach similar to that shown in Fig. 4, G and G_c are computed *a posteriori* and the contours of ΔG are plotted in Fig. 9. Since the cost functional cannot be reduced to zero exactly, the quasi-direct validation solution produces certain regions with positive ΔG along the interface when $\delta = 0$ is used in Eq. (19) while seeking a marginal stability solution (Fig. 9). A nonzero δ solution reduces the previously (i.e., with $\delta = 0$) obtained ΔG by a certain amount. Whether this amount is enough to overcome the appearance of positive ΔG at all times (except near $t = t_{max}$) depends on the accuracy that has been reached in the optimization scheme. A heat flux solution $q_{o\ell}(y, t)$ from relatively larger δ

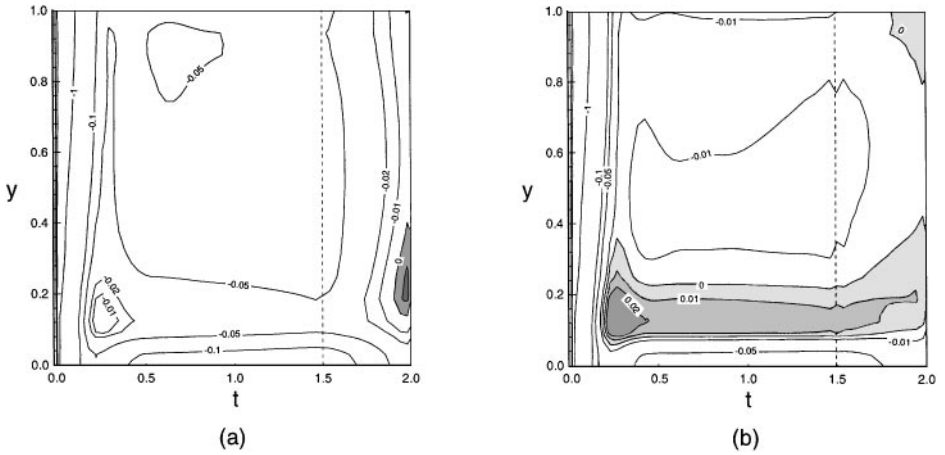

FIG. 9. Contours of ΔG corresponding to the optimum $\hat{q}_{o\ell}(y,t)$: (a) $\delta = 0.2$: $\Delta G < 0$ which implies that a stable interface is achieved for most of the times, except for a small region (shaded) near $t = t_{\max}$. The existence of this region is due to the fact that $\epsilon(t_{\max}) = 0$ from $\mathbf{v}_f(t_{\max}) = 0$ even though $\delta \neq 0$; (b) $\delta = 0$; a stripe (shaded) centering near the interface location $y = 0.12$ has $\Delta G > 0$ (unstable), while the bottom part of the interface is always "over stable." Because of the convective effects, $y \sim 0.12$ represents the location around which constitutional instability will develop. Note that up to time $t \sim 0.15$ and due to the initial high interface temperature gradient, a stable growth is observed. The maximum deviation from the stability conditions is observed at $t \sim 0.3$.

can lead to a stable interface growth even though it is one that has not reached very small values of the cost functional in the CGM iterations.

Representative transient temperature, concentration, and flow fields (contour lines of isotherms, isopleths, and stream functions) of the quasi-direct validation problem are displayed in Fig. 10, under the boundary heat flux $\hat{q}_{o\ell}$ that leads to stable growth. Because of such a heating flux at $x = 0.5$, a horizontal temperature gradient is maintained up to time $t_{mid} = 1.5$. This is the key mechanism that allows the thermal gradient at the interface to overcome the intrinsic concentration gradient due to solute rejection and thus to lead to a stable growth. Since $Pr > 1$, the maximum strength of convection is established at an early stage ($t \sim 0.3$). For the current choice of Ra_T/Ra_C and geometry, only one major convection cell appears whose strength is significantly reduced after time t_{mid}. Since the solute diffusivity is small, the convective flow strength controls the magnitude of the curvature of the isopleths near the interface; $y = 0.12$ turns out as the location on the interface with maximum concentration gradients, and thus, closest to conditions of marginal stability. This explains our earlier observations in Fig. 9.

In Fig. 11, we record the spatial-temporal history of the interface temperature as calculated from the quasi-direct validation solution. From Eq. (14) and the phase diagram Fig. 2, we know that the contours of Fig. 11b also provide a representation of the pattern of solute distribution in the final solidified product. The spatial nonuniformity of the solute distribution is induced by convection flow effects and is sensitive to the growth velocity variations (note that the isotherms change directions after $t_{mid} = 1.5$ when $\boldsymbol{v}_f$ starts to decrease).

The solution $\hat{q}_{os}(y,t)$ of the inverse heat conduction problem in the solid region is shown in Fig. 12. It is obtained by the adjoint method, using the interface heat flux and temperature in Fig. 11a from the quasi-direct validation problem with $\delta = 0.2$. Additional

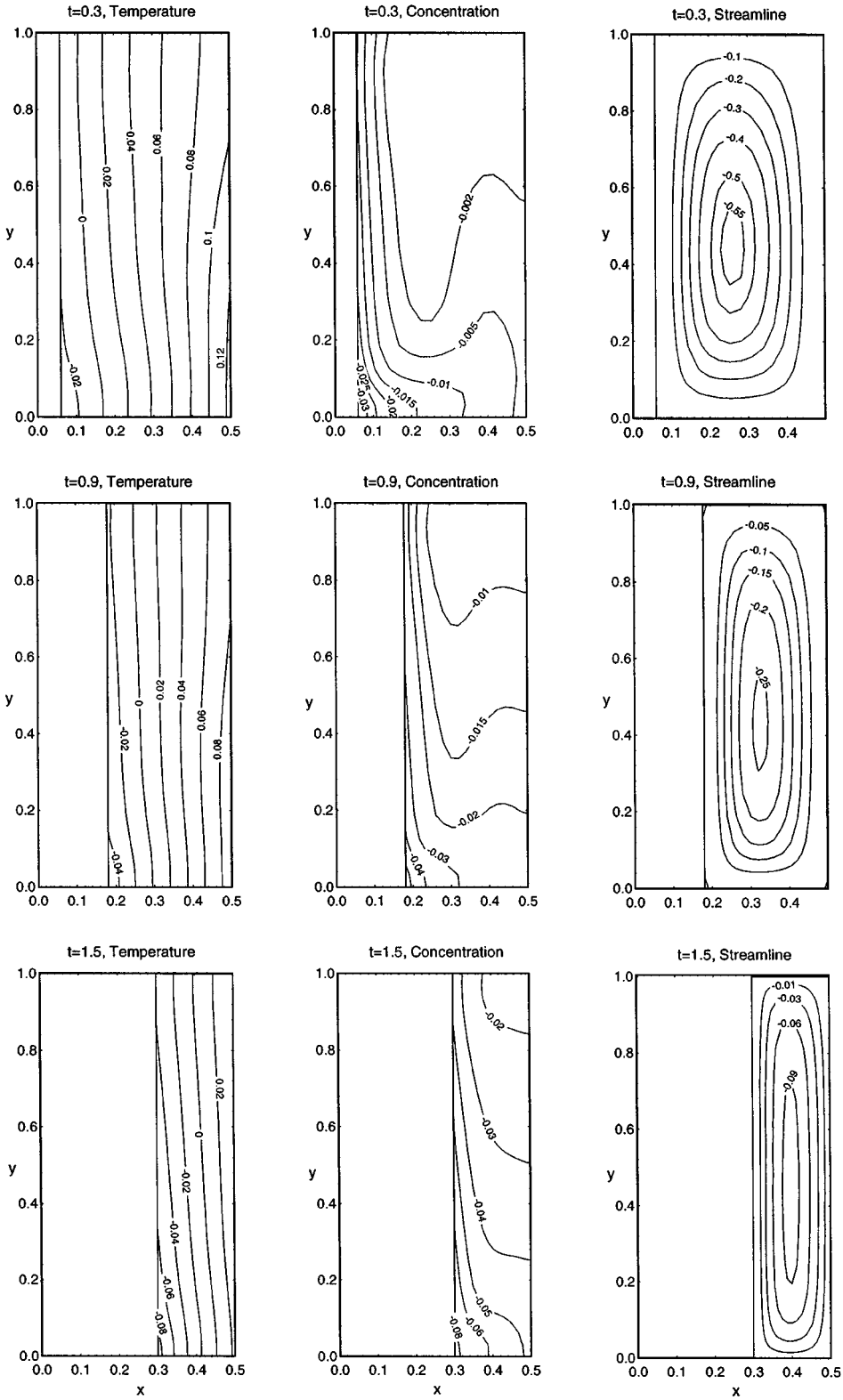

FIG. 10. Temperature, concentration, and flow fields from the validation solution ($\delta = 0.2$).

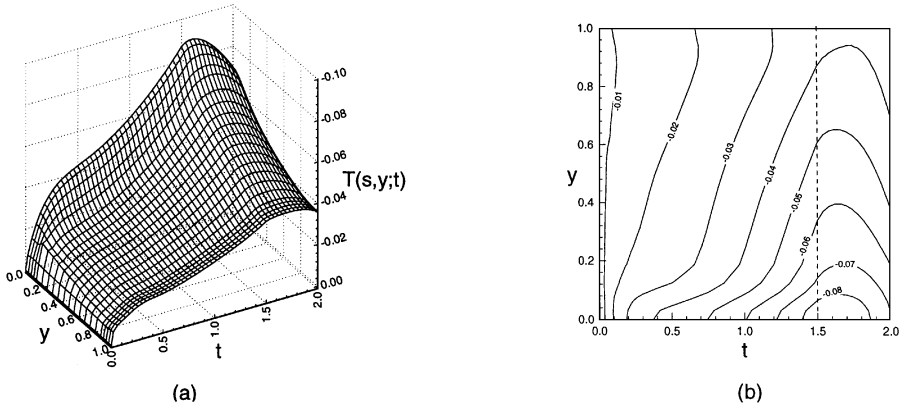

FIG. 11. Interface temperature $T(s, y; t)$ from validation solution ($\delta = 0.2$): (a) history; (b) contours of isotherms in the (y, t) plane.

nondimensional parameters involved are $R_k = R_\alpha = 1$ and $Ste = 0.3$. Its combination with $\hat{q}_{o\ell}$ from Fig. 7b provides the complete solution that leads to a stable interface growth as described by Eqs. (51) and (52).

5. CONCLUSIONS

In this work, a systematic continuum formulation of the adjoint method is proposed to solve an inverse thermo-solutal convection problem. The objective is to control the boundary heating/cooling fluxes such that solidification of dilute binary alloys proceeds with a desired stable interface growth. Such study identifies possible inconsistencies in the previous binary alloy solidification models that a-priori assume a macroscopically sharp solid/liquid interface. The stability criterion was here chosen as the absence of constitutional undercooling in the liquid ahead of the interface. Such relation of the interface stability is treated as an overspecified boundary condition in the inverse problem formulation. Based on additional physical arguments of marginal stability and minimum energy input, the

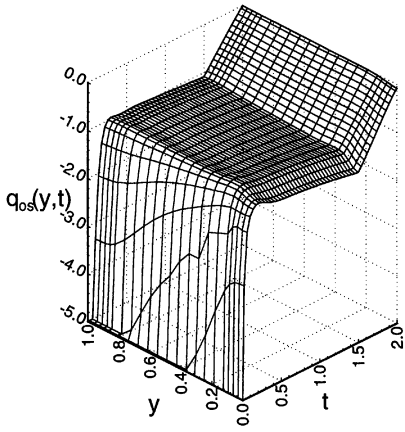

FIG. 12. Optimum heat flux $q_{os}(y, t)$ at solid mold wall.

constitutional undercooling condition is implemented in the form of an equality. We define the cost functional as the thermal deviation of the freezing interface from thermodynamic equilibrium. The inverse design problem is posed as the calculation of the optimum boundary heat flux that leads to the minimization of the cost functional. A close form of the adjoint equation system is derived with coupled thermal, solute, and flow transport mechanisms. The definition of the adjoint system is made such that the boundary value of the adjoint thermal variable at the fixed wall is equal to the gradient of the cost functional. The conjugate gradient algorithm is used to solve for the optimum boundary heat flux that minimizes the cost functional. Since such a heat flux is a function varying in space and time, the adjoint method provides an elegant and efficient numerical scheme for the solution of this class of problems. An example case of the solidification of NH_4Cl water solution in a rectangular cavity is performed for moderate strength of thermo-solutal convection. Introduction of small amount of "over-stability" is introduced to overcome the problem of loss of stability because of the accuracy level that the numerical optimization scheme can reach.The results are validated to show the achievement of a stable vertical flat freezing interface growth at the desired growth velocity.

The algorithm for an accurate solution of the inverse thermo-solutal convection problem is computationally intensive. Further parametric studies and improvement of the formulation are needed for systems with larger Rayleigh and Lewis numbers. Such studies can extend the applicability of the current algorithm to the solidification of semiconductor materials and metallic alloys and to processes with stronger melt convection. There is a great potential in improving the convergence of the CGM by other techniques such as regularization and preconditioning. Finally, we should note that the design choice of the boundary heat flux may not be sufficient to control such complex systems with coupled transport mechanisms. Additional means such as forced convection through electro-magnetic stirring or rotation may be necessary for the design of alloy solidification processes. In addition, solidification with force convection and boundary heating/cooling design may lead to processes that in addition to stable growth lead to the minimization of solute segregation and reduction of various solidification defects. A significant number of analytical and computational issues in this direction remain to be addressed.

ACKNOWLEDGMENTS

The results presented in this paper were obtained in the course of research sponsored by the National Science Foundation under a PYI Award DDM-9157189 and Grant CTS-9115438 to Cornell University and with support from Alcoa Laboratories. The partial support of the senior author by the Air Force Office of Scientific Research through the VPI-Cornell Center for PDE Optimization and Control is acknowledged. The computing for this project was supported by the Cornell Theory Center, which receives major funding by the NSF and IBM Corporation, with additional support from the New York State.

REFERENCES

1. J. Hadamard, Sur les problem aux derivees partielles at leur signification physique, *Bull. Univ. Princeton* **13**, 49 (1902).
2. A. N. Tikhonov, *Solutions of Ill-Posed Problems* (Halsted Press, Washington, 1977).
3. D. A. Murio, *The Mollification Method and the Numerical Solution of Ill-Posed Problems* (Wiley, New York, 1993).

4. J. V. Beck, B. Blackwell and C. R. St. Clair, Jr., *Inverse Heat Conduction, Ill-posed Problems* (Wiley-Interscience, New York, 1985).
5. O. M. Alifanov, *Inverse Heat Transfer Problems* (Springer-Verlag, Berlin, 1994).
6. P. Neittaanmäki and D. Tiba, *Optimal Control of Nonlinear Parabolic Problems* (Marcel Dekker, New York, 1994).
7. N. Zabaras, Y. Ruan and O. Richmond, On the design of two-dimensional Stefan processes with desired freezing front motions, *Numer. Heat Transfer* **21**(B), 307 (1992).
8. N. Zabaras, Inverse finite element techniques for the analysis of solidification processes, *Int. J. Numer. Methods Engr.* **29**, 1569 (1990).
9. N. Zabaras and S. Kang, On the solution of an ill-posed inverse design solidification problem using minimization techniques in finite and infinite dimensional spaces, *Int. J. Numer. Methods Engr.* **36**, 3973 (1994).
10. S. Kang and N. Zabaras, Control of the freezing interface motion in two-dimensional solidification processes using the adjoint method, *Int. J. Numer. Methods Engr.* **38**, 63 (1995).
11. N. Zabaras and T. Hung Nguyen, Control of the freezing interface morphology in solidification processes in the presence of natural convection, *Int. J. Numer. Methods Engr.* **38**, 1555 (1995).
12. Y. Jarny, M. N. Özisik and J. P. Bardon, A general optimization method using adjoint equation for solving multidimensional inverse heat conduction, *Int. J. Heat Mass Transfer* **34**(11), 2911 (1991).
13. A. Moutsoglou, An inverse convection problem, *J. Heat Transfer ASME* **111**, 37 (1989).
14. P. Cuvelier, Optimal control of a system governed by the Navier–Stokes equations coupled with the heat equations, in *New Developments in Differential Equations* (W. Eckhaus, Ed.) (North-Holland, Amsterdam, 1976), p. 81.
15. M. D. Gunzburger, L. Hou and T. Svobodny, Heating and cooling control of temperature distributions along boundaries of flow domains, *J. Math. Syst. Estim. Control* **3**(2), 147 (1993).
16. M. D. Gunzburger and H. C. Lee, Analysis, approximation, and computation of a coupled solid/fluid temperature control problem, *Comp. Methods Appl. Mech. Engr.* **118**, 133 (1994).
17. N. Zabaras and G. Yang, A functional optimization formulation and FEM implementation of an inverse natural convection problem, *Comp. Methods Appl. Mech. Engr.* **144**(3–4), 245 (1997).
18. G. Yang and N. Zabaras, Adjoint methods for the design of solidification processes with natural convection, *Int. J. Numer. Methods Engr.*, submitted.
19. W. Kurz and D. J. Fisher, *Fundamentals of Solidification* (Trans Tech Publications Ltd, Switzerland, 1989).
20. M. E. Thompson and J. Szekely, Mathematical and physical modelling of double diffusive convection of aqueous solutions crystallizing at a vertical wall, *J. Fluid Mech.* **187**, 409 (1988).
21. S. R. Coriell and G. B. McFadden, Morphological stability, Chapter 12 in *Handbook of Crystal Growth, Fundamentals: Transport and Stability*, Vol. 1b (D. T. J. Hurle, ed.), p. 785.
22. W. D. Bennon and F. P. Incropera, A continuum model for momentum, heat and species transport in binary solid-liquid phase change systems—II. Application to solidification in rectangle cavity, *Int. J. Heat Mass Transfer* **30**(10), 2171 (1987).
23. A. N. Brooks and T. J. R. Hughes, Streamline upwind/Petrov-Galerkin formulations for convection dominated flows with particular emphasis on the incompressible Navier-Stokes equations, *Comp. Methods Appl. Mech. Engr.* **32**, 199 (1982).
24. J. C. Heinrich, A finite element model for double diffusive convection, *Int. J. Numer. Methods Engr.* **20**, 447 (1984).
25. G. Z. Yang, *The Adjoint Method for the Inverse Design of Solidification Processes with Convection* (Ph.D. Dissertation, Sibley School of Mechanical and Aerospace Engineering, Cornell University, Ithaca, NY, August 1997).
26. R. Fletcher, *Practical Methods of Optimization* (Wiley-Interscience, New York, 1987).
27. D. G. Luenberger, *Optimization by Vector Space Methods* (Wiley-Interscience, New York, 1968).